Rare Metal Materials and Engineering
Volume 52, Issue 1, January 2023
Available online at www.rmme.ac.cn

Science Press

Cite this article as: Wu Yanxia, Chen Yufeng, Liang Hailong, et al. Effect of Sn Doping on Alkali Metal Resistance of V/UiO-66 Catalyst[J]. Rare Metal Materials and Engineering, 2023, 52(01): 41-47.

ARTICLE

Effect of Sn Doping on Alkali Metal Resistance of V/UiO-66 Catalyst

Wu Yanxia, Chen Yufeng, Liang Hailong, Hu Liming, Wang Chunpeng

Ceramics Science Institute, China Building Materials Academy, Beijing 100024, China

Abstract: V/UiO-66 catalyst and modified Sn-V/UiO-66 catalyst were prepared by impregnation method with UiO-66 as carrier, and their potassium poisoning was simulated. The reaction and deactivation mechanisms of vanadium-titanium catalyst were analyzed. Results demonstrate that the crystallographic form of catalysts barely changes after K-loading, and the specific surface area of the catalysts has an irregular fluctuation. The catalyst activity is decreased rapidly after the alkali metal was loaded due to the degraded metal redox performance and the rapidly decreased surface acid content of the catalysts. The addition of Sn can enhance the interaction between VO_x and other components, which thereby increases the V^{5+} content and reducibility of VO_x. Thus, VO_x on the surface of Sn-V/UiO-66 catalysts can provide more acid sites. The poisoned K-Sn-V/UiO-66 catalyst still has high total acid content and strong redox property, presenting the high resistance of Sn-V/UiO-66 catalyst against alkali metal poisoning.

Key words: UiO-66 catalyst; catalytic denitration; NH_3-SCR; modification

Nitrogen oxides are one of the primary sources of air pollution caused by the combustion of fossil materials[1], which causes environmental problems, such as photochemical smog, acid rain, greenhouse effect, and serious health problems[2–5]. Therefore, reducing nitrogen oxides becomes the primary goal of environmental protection. Currently, the ammonia selective catalytic reduction (NH_3-SCR) is a mature and the most widely used method for stationary source denitrification[6–8]. Through catalyst, the reducing agent converts the nitrogen oxides in gas into harmless nitrogen and water. The cost of catalysts usually accounts for 30%–40% of the total cost.

In the selective catalytic reduction (SCR) reactor, there are two main types of arrangement: high-dust and low-dust. In the high-dust environment, SCR reactor is placed at the downstream of the economizer and the upstream of the air preheater with the flue gas temperature of approximately 350 °C. In the low-dust environment, SCR reactor is located behind the desulfurization and dust removal devices. The most widely used high-dust SCR catalyst is V_2O_5-$MoO_3(WO_3)/TiO_2$ because its active temperature is 300–400 °C[9–10]. Nevertheless, the high-dust environment contains many toxic substances, including Na, K, Ca, and As, which can poison the catalysts and degrade their performance.

The poisoning effects of alkali metals on catalysts have been extensively researched. Generally, it is believed that Na and K poisoning is a chemical poisoning: Na and K occupy the acid sites on the catalyst surface and reduce the NH_3 adsorption capacity, thereby reducing SCR activity[11–13]. CaO poisoning, as a physical poisoning, is caused by the generation of $CaSO_4$ and the blocking of catalyst micropores[14–15]. Among the alkali metals in the flue gas, K has the most severe effect on the catalyst. Therefore, it is necessary to improve the anti-alkali metal poisoning ability of catalysts and to prolong the service life of catalysts. The provision of more sacrificial acid sites and the establishment of capture sites to protect active sites are the main solutions[16–18]. It is demonstrated that the Sn oxides exhibit unique electrochemical and chemical properties, which can improve the redox performance of catalysts at low temperatures and control the acidity of catalyst substrates[19].

The active substance Sn was added to the V/UiO-66 catalyst in this research, and the anti-alkali metal poisoning ability of catalysts was improved by increasing the acid sites and enhancing the surface oxidation performance.

Received date: April 07, 2022
Foundation item: National Key Research and Development Program of China (2016YFC0209302)
Corresponding author: Wu Yanxia, Candidate for Ph. D., Engineer, Ceramics Science Institute, China Building Materials Academy, Beijing 100024, P. R. China, Tel: 0086-10-51167727, E-mail: wuyanxia@cbma.com.cn

Copyright © 2023, Northwest Institute for Nonferrous Metal Research. Published by Science Press. All rights reserved.

1 Experiment

An appropriate amount of ammonium metavanadate (NH_4VO_3) was dissolved in hot water at 90 °C. Then the monoethanolamine was added dropwise until a transparent solution was obtained. When the mixture was cooled down to room temperature, UiO-66 without and with stannous sulfate was separately added into the solution and mixed thoroughly. After drying at 105 °C for 12 h and calcining at 350 °C for 3 h, the catalysts with 3wt% V_2O_5/UiO-66 and those with 1wt% SnO_2/UiO-66 were obtained, which were named as V/UiO-66 and V-Sn/UiO-66 catalysts, respectively.

The impregnation method was used to simulate the K-poisoning of catalysts. The K_2SO_4 solution with molar ratio of K:V=2:1 was prepared. The prepared catalysts were immersed in K_2SO_4 solution for 5 h, then dried at 105 °C for 8 h, and calcined at 350 °C for 4 h. The poisoned catalysts were named as K-V/UiO-66 and K-V-Sn/UiO-66 catalysts.

The X-ray diffractometer (XRD, D8 advanced XRD by Bruker, Germany) was used for catalyst characterization. The current was 40 mA, the voltage was 40 kV, Cu Kα was used as the radiation source, and the scanning range was 2θ=10°~80° with the scanning step of 0.02°.

The N_2 physical adsorption test of the catalyst was performed by the Autosorb-iQ physical adsorption instrument (Quantachrome Company, United States). The catalyst specimens of 0.25–0.3 g were pretreated by vacuuming at 240 °C for 2 h and then placed in liquid nitrogen (−196 °C) for tests. The specific surface area was calculated by the Brunauer-Emmett-Teller (BET) method.

The H_2-temperature programmed reduction (TPR) of the catalysts was conducted by Auto Chem II 2920 Chemisorber (Mack Co., Ltd). The specimen (50 mg, particle size of 0.30–0.45 mm) was pretreated in pure Ar atmosphere at 300 °C for 0.5 h. The temperature rose from 50 °C to 800 °C at a heating rate of 10 °C/min in the atmosphere of 10vol% H_2/Ar with flow rate of 20 mL/min. The thermal conductivity detector (TCD) was used to measure the consumption of H_2 in this process.

The NH_3-temperature programmed desorption (TPD) of the catalysts was conducted by Auto Chem II 2920 Chemisorber (Mack Co., Ltd). The specimen (100 mg, particle size of 0.30–0.45 mm) was pretreated in a pure He atmosphere (flow rate of 20 mL/min) at 400 °C for 0.5 h. After cooling to 50 °C, 5vol% NH_3/N_2 with flow rate of 20 mL/min was introduced to adsorb NH_3 for 0.5 h. Then, the pure He was purged for 1 h. Finally, the temperature rose to 500 °C with heating rate of 10 °C/min. TCD was used to measure the desorbed NH_3 content during this process.

The catalysts were characterized by X-ray photoelectron spectroscope (XPS, Thermo Scientific ESCALAB 250Xi). The vacuum degree of the analysis chamber was 8×10^{-10} Pa, the excitation source was Al Kα ($h\nu$=1253.6 eV), the working voltage was 12.5 kV, the filament current was 16 mA, and the signal accumulation was conducted for 10 cycles.

The activity evaluation of the catalyst was conducted in a stainless-steel SCR fixed reactor with external heating in a tube furnace. The schematic diagram of experiment setup is shown in Fig.1. The simulated gas composition was 0.05vol% NO, 0.05vol% NH_3, 6.00vol% O_2, and N_2 (equilibrium carrier gas). The catalyst amount was 5 mL, the total gas flow was 1000 mL/min, and the space velocity was 12 000 h^{-1}. The catalyst activity was evaluated at 100–340 °C, and the NO content before and after the reaction was detected by German Testo 350 flue gas analyzer. The NO removal rate η is calculated by Eq.(1), as follows:

$$\eta=\frac{V_{\text{NO-in}}-V_{\text{NO-out}}}{V_{\text{NO-in}}}\times100\% \quad (1)$$

where $V_{\text{NO-in}}$ is the volume of ingoing NO gas and $V_{\text{NO-out}}$ is the volume of outgoing NO gas.

2 Results and Discussion

2.1 XRD analysis of catalysts

Fig.2 illustrates XRD patterns of different catalysts. Typical diffraction peaks of tetragonal ZrO_2 can be observed at 2θ= 29.7°, 34.6°, 49.6°, and 59.2° of all catalysts, and the corresponding crystal plane are (003), (012), (104), and (113), respectively[20]. The diffraction peaks of vanadium oxide and tin oxide cannot be observed. There are three possible reasons for this phenomenon: (1) the contents of vanadium oxide and tin oxide are low; (2) the diffraction peaks of vanadium oxide and tin oxide are covered by ZrO_2 diffraction peaks; (3) the vanadium oxide and tin oxide are uniformly dispersed on the carrier surface in the amorphous. Comparing the V/UiO-66 and Sn-V/UiO-66 catalysts, it can be seen that the peak intensity of the crystal phase is weakened after Sn addition into the V/UiO-66 catalyst, indicating a strong interaction between the active component and the substrate. Thus, Sn^{4+} is distributed randomly in the ZrO_2 lattice, reducing the crystallinity and size of ZrO_2 carrier particles. Furthermore, the number of electrons and oxygen vacancies increases, which also improves the reactions[21].

The diffraction peak of K_2SO_4 cannot be observed in the K-V/UiO-66 and K-Sn-V/UiO-66 catalysts, indicating that the K content is low. In addition, K element is mainly distributed in a monolayer state and highly dispersed on the catalyst carrier surface. Besides, the diffraction angle and peak intensity barely change after K_2SO_4 is loaded, which suggests that the alkali metal loading does not significantly impact the crystal structure of catalyst. Therefore, the reduction in catalyst

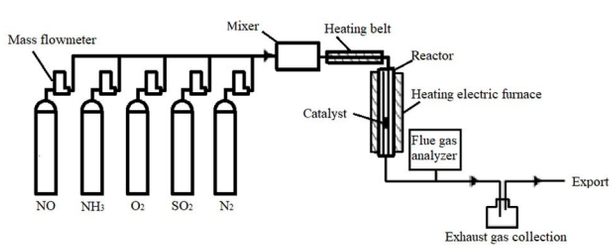

Fig.1 Schematic diagram of experiment device for catalyst activity evaluation

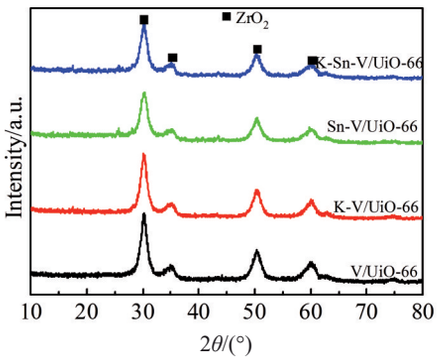

Fig.2 XRD patterns of different catalysts

denitration activity after K-poisoning is not directly related to the crystal phases of catalysts.

2.2 BET analysis of catalysts

Table 1 shows the BET specific surface area of V/UiO-66, Sn-V/UiO-66, K-V/UiO-66, and K-Sn-V/UiO-66 catalysts. The Sn-V/UiO-66 catalyst has the specific surface area of 220.87 $m^2 \cdot g^{-1}$, which is approximately 2.4 times greater than that of the V/UiO-66 catalyst (93.16 $m^2 \cdot g^{-1}$), indicating that the Sn addition significantly increases the specific surface area of catalyst. It is also observed that the Sn^{4+} gathers at the grain boundary of UiO-66. It is worth noting that due to the similar ionic radii of Sn^{4+} (0.069 nm) and Zr^{4+} (0.072 nm), a large number of Sn ions are inserted into the UiO-66 lattice, replacing some Zr^{4+} ions and thereby forming a novel skeleton structure. The smaller radius of Sn^{4+} ions results in the inhabitation of particle growth by reducing the grain boundary energy. Consequently, the specific surface area of specimen increases after Sn doping[22]. The NH_3-SCR reaction occurs at the catalyst surface. It is believed that the high specific surface area of the catalyst can provide more active adsorption centers for the reaction molecules and intermediate products in the gas-solid reaction, which effectively promotes the phase transfer, therefore enhancing the denitrification activity of the catalysts[23].

It is found that after K-poisoning, the specific surface area of catalyst becomes smaller, because the alkali metal salt particles are distributed on the catalyst surface and some pores are blocked. The specific surface area of the V/UiO-66 catalyst is 93.16 $m^2 \cdot g^{-1}$, whereas that of the K-V/UiO-66 catalyst is 95.99 $m^2 \cdot g^{-1}$, indicating that the specific surface area is slightly increased by the K-poisoning. However, for the Sn-V/UiO-66 catalyst, the specific surface area is decreased from 220.87 $m^2 \cdot g^{-1}$ to 165.80 $m^2 \cdot g^{-1}$ after K-poisoning. This result suggests that the K-poisoning leads to the reduction in specific surface area of catalysts. It can be observed that the specific surface area of the catalyst fluctuates after K loading[24]. However, the catalyst activity does not change significantly.

Table 1 BET specific surface area of different catalysts ($m^2 \cdot g^{-1}$)

V/UiO-66	Sn-V/UiO-66	K-V/UiO-66	K-Sn-V/UiO-66
93.16	220.87	95.99	165.80

2.3 H_2-TPR analysis of catalysts

H_2-TPR tests were used to characterize the effect of alkali metals on the redox ability of catalysts. Fig. 3 shows the H_2-TPR curves of different catalysts. It is known that the dispersed and multimeric vanadium oxides undergo a multi-step reduction process of $V^{5+} \rightarrow V^{4+} \rightarrow V^{3+} \rightarrow V^{2+}$ at 400–600 °C. The superimposed reduction peaks of vanadium oxides occur at 400 and 550 °C[25]. Compared with the V/UiO-66 catalyst, the K-Sn-V/UiO-66 catalyst exhibits a greater reduction peak area and its peak shifts towards the lower temperature area. With Sn addition, the interaction between Sn and Zr increases the redox ability of the catalyst and facilitates the reduction of V-O component. The redox properties of catalysts play a significant role. In addition, the lower the reduction initiation temperature of the catalyst, the stronger the redox ability of the catalyst[26]. Combined with the NH_3-SCR results of catalyst activity, it can be seen that the Sn-V/UiO-66 catalyst with strong redox performance exhibits better catalytic activity than the V/UiO-66 catalyst with poor redox performance does. This result suggests that the redox property determines the catalyst activity in a significant manner.

Compared with the V/UiO-66 catalyst, the center temperature of the reduction peak shifts to the higher temperature area for the K-V/UiO-66 catalyst. According to Ref. [27], the catalyst reducibility depends on the grain arrangement and grain structure of catalyst. The K-poisoning causes the rearrangement of crystals due to the interactions between K and complex oxides. The poor alignment state results in the poor reducibility of catalyst, as indicated by the shifting of the peak temperature towards the high temperature area. This phenomenon also infers that the activity of surface oxides is significantly reduced after K-poisoning. Thus, the VO_x can hardly be reduced and the redox performance of catalyst is reduced, which affects the SCR process, such as NH_3 activation and NO oxidation. Therefore, the Sn doping can improve the redox performance of V/UiO-66 catalyst and effectively protect the catalyst from K-poisoning.

2.4 NH_3-TPD analysis of catalysts

The surface acidity of catalyst evaluated by NH_3-TPD process can significantly influence the NH_3-SCR reaction[25].

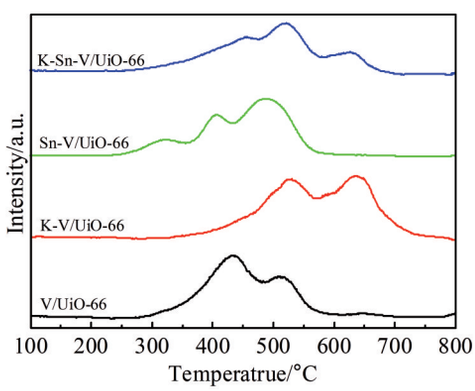

Fig.3 H_2-TPR curves of different catalysts

Fig.4 shows the NH_3-TPD curves of different catalysts. It can be seen that the NH_3-TPD curve of V/UiO-66 catalyst has a prominent NH_3 desorption peak at 75−150 °C. After adding Sn, the Sn-V/UiO-66 catalyst shows two NH_3 desorption peaks at 75−150 and 375−425 °C, which are attributed to the desorption of NH_4^+ at the Brønsted acid site and the desorption of NH_3 at the Lewis acid site[28], respectively. Compared with the NH_3 at Lewis acid sites, NH_4^+ at Brønsted acid sites is more unstable and more prone to desorption. Fig.4 also shows that the Sn-V/UiO-66 catalyst has a larger desorption peak area than the V/UiO-66 catalyst does. This phenomenon indicates that the Sn addition can increase the number of Brønsted acid sites and Lewis acid sites on the catalyst surface to a certain extent, which is beneficial to the adsorption and activation of NH_3[29].

When alkali metals are loaded on the catalyst, the acid content decreases rapidly, especially for the V/UiO-66 catalyst. This result is consistent with the results in Ref.[30]. It is reported that the potassium can affect both the Lewis acid and Brønsted acid on the catalyst surface, i.e., the number and strength of acid sites are reduced by K-poisoning. This is mainly because in SCR catalyst, V-OH exists as the Brønsted acid site, providing the active acid sites for SCR reactions; the reducing agent NH_3 is adsorbed on these active sites, thereby promoting the activation and removal of NO. After the alkali metal is loaded, K preferentially adsorbs on the acid sites on catalyst surface and combines with the V element to form V-O-K components, which hinders the adsorption of NH_3 on the Brønsted acid site, thereby reducing the surface acidity. The decreased Lewis acid may be related to the reduction in the specific surface area of the catalyst, and it is speculated that the alkali metal compounds occupy or cover some active sites. The surface acidity of catalyst significantly influences the NH_3 adsorption amount. K-poisoning reduces the surface acidity of the catalyst, therefore decreasing the SCR activity of the catalyst. It is worth noting that the total acid content of the poisoned K-Sn-V/UiO-66 catalyst is higher than that of the V/UiO-66 catalyst, indicating that the Sn addition can effectively reduce the effect of K-poisoning on the surface acidity of catalyst. In brief, the Sn addition can provide abundant acid sites for the catalyst and improve the anti-alkali metal poisoning property of catalyst.

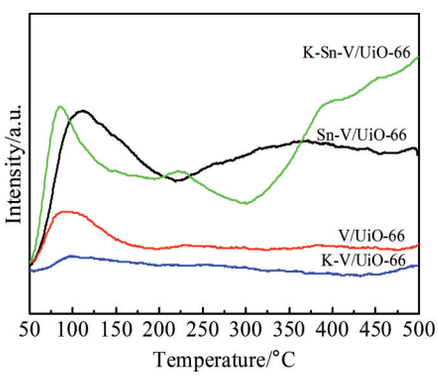

Fig.4 NH_3-TPD curves of different catalysts

2.5 XPS analysis of catalysts

The surface properties of the catalyst are crucial to the catalytic reaction. Fig.5a shows the overall XPS spectra of the surfaces of different catalysts. As for the V/UiO-66 and Sn-V/UiO-66 catalysts, C 1s, V 2p, Zr 3d, O 1s, and Sn 3d peaks can be observed according to their XPS spectra. As for the K-

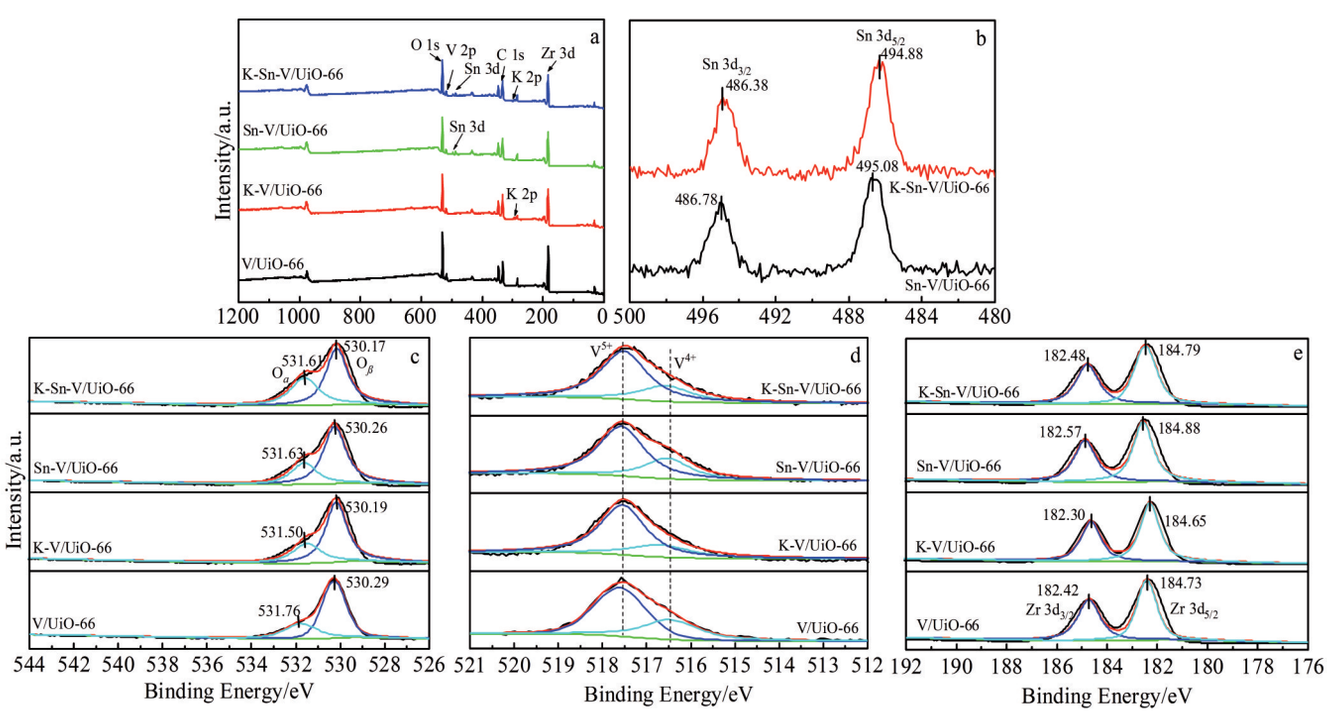

Fig.5 XPS spectra of different catalysts: (a) overall spectra; (b) Sn 3d; (c) O 1s; (d) V 2p; (e) Zr 3d

V/UiO-66 and K-Sn-V/UiO-66 catalysts, K 2p peak can be observed. The low peak intensity of K 2p is related to the small content of K_2SO_4 on the catalyst surface.

Fig.5b shows XPS spectra of Sn 3d of Sn-V/UiO-66 and K-Sn-V/UiO-66 catalysts. It can be seen that the Sn 3d spectra contain two peaks: Sn $3d_{3/2}$ and Sn $3d_{5/2}$. For the Sn-V/UiO-66 catalyst, the binding energies of Sn $3d_{3/2}$ and Sn $3d_{5/2}$ peaks are 486.78 and 495.08 eV, respectively, which indicates that Sn exists as Sn^{4+} in the Sn-V/UiO-66 catalyst. After K_2SO_4 is deposited on Sn-V/UiO-66 catalyst, the binding energy of Sn 3d shifts to the lower binding energy area, and the decrease range is within 0.4 eV. The deposition of K_2SO_4 on Sn-V/UiO-66 does not change the oxidation state of Sn, and Sn still exists as SnO_2.

Fig. 5c shows XPS spectra of O 1s of different catalysts. The binding energy of lattice oxygen (O^{2-}, denoted as O_β), is 530.1 – 530.3 eV, and that of the adsorbed oxygen (O^-/O_2^{2-}, denoted as O_α) on catalyst surface is 531.5 – 531.8 eV. According to Ref. [31], the adsorbed oxygen on catalyst surface is considered as the main surface-active oxygen components due to its high mobility, therefore playing an essential role in oxidation reactions. High O_α content leads to the strong oxidization ability, thereby promoting the NO oxidation into NO_2 and the rapid SCR reaction. It can be seen from Table 2 that the adsorbed oxygen content on the surface of V/UiO-66 catalyst is 29.83%, and that of the Sn-V/UiO-66 catalyst is 30.44%. After adding Sn, the adsorbed oxygen content of the catalyst is slightly increased.

After K-poisoning, the adsorbed oxygen content on the surface of V/UiO-66 catalyst changes slightly from 29.83% to 31.08%, while that of the Sn-V/UiO-66 catalyst increases from 30.44% to 39.54%. The surface-active oxygen significantly increases, resulting in the specific reactivity of K-Sn-V/UiO-66 catalyst. In addition, the binding energy of O 1s in catalysts after K-poisoning shifts to the lower energy area, which indicates that K coordinates with V in the catalyst and occupies the V-OH and V=O active sites on the catalyst surface to form V-O-K components, thereby increasing the electron cloud density in the outer valence electron layer of the oxygen nucleus.

Fig. 5d illustrates XPS spectra of the V 2p of different catalysts. The binding energy of V^{4+} is 516.5 – 516.7 eV, and that of V^{5+} is 517.5 – 517.7 eV. For the vanadium-based catalysts, the redox cycle between V^{4+} and V^{5+} is crucial for the catalytic activity. In SCR reaction, V^{4+} and V^{5+} on the catalyst surface mainly exist in the form of V-OH and V=O, respectively. NO in the flue gas is oxidized into NO_2, and V^{5+}=O is reduced to V^{4+}-OH, which promotes the fast SCR reaction and improves the low-temperature activity of the catalyst. Metastable V^{4+} can promote the occurrence of this cyclic transition[27]. The proportion of V^{4+} in the Sn-V/UiO-66 catalyst is 29.51at%, which is lower than that in the V/UiO-66 catalyst (35.47at%), as shown in Table 3. It is speculated that after adding Sn, Sn^{4+} oxidizes partial low-valence V^{4+} into high-valence V^{5+} . After K-poisoning, for the V/UiO-66 catalyst, the proportion of V^{4+} decreases from 35.47at% to 25.04at%. The decrease in V^{4+} content inevitably leads to the significant reduction in the activity of SCR reaction.

Fig.5e illustrates XPS spectra of Zr 3d in different catalysts. The binding energy of Zr $3d_{5/2}$ is 184.6–184.9 eV, while that of Zr $3d_{3/2}$ is 182.3–182.6 eV. Zr element mainly exists as Zr^{4+} on the ZrO_2 surface[32]. As shown in Fig.5, the binding energies of Zr $3d_{5/2}$ and Zr $3d_{3/2}$ in V/UiO-66 catalyst are 184.73 and 182.42 eV, respectively. After Sn addition, the binding energies of Zr $3d_{5/2}$ and Zr $3d_{3/2}$ in Sn-V/UiO-66 catalyst are increased to 184.88 and 182.57 eV, respectively. This result indicates that the binding energy of Zr surface increases, the interaction between the catalyst and the active components is enhanced, and therefore the denitration activity is improved. After K-poisoning, the binding energy of Zr $3d_{5/2}$ in V/UiO-66 catalyst decreases from 184.73 eV to 184.65 eV, and that of Zr $3d_{3/2}$ decreases from 182.42 eV to 182.30 eV. Therefore, the decrease in denitrification activity is caused by the reduced interactions between catalyst and active components due to the K-poisoning.

2.6 Denitration performance test of catalyst

Fig. 6 shows the denitration activity curves of different catalysts. It can be seen that the denitrification activity of V/UiO-66 and Sn-V/UiO-66 catalysts is increased with increasing the temperature, and the highest efficiency approaches 100% within a wide temperature range. The temperature window of V/UiO-66 catalyst is 180 – 340 °C, while that of Sn-V/UiO-66 catalyst is 160–340 °C. Therefore, the temperature window extends slightly to the low-temperature area after the Sn modification. After K-poisoning, the SCR activity of the V/UiO-66 catalyst decreases significantly, and the highest NO conversion ratio decreases from 100% to 60%. Although the activity of Sn-V/UiO-66 catalyst also reduces to a certain extent, the NO conversion ratio, namely NO removal ratio, is still more than 80% at 200–340 °C. Therefore, Sn doping significantly enhances the resistance of catalyst against alkali metal K-poisoning.

2.7 Discussion

According to the Lewis acid mechanism, SCR reaction process is as follows:

$$NH_3+V^{5+}+O^{2-}\rightarrow V^{4+}\cdots NH_2+OH^- \quad (2)$$

Table 2 Oxygen contents on different catalyst surfaces (%)

Catalyst	O_α	O_β
V/UiO-66	29.83	70.17
K-V/UiO-66	31.08	68.92
Sn-V/UiO-66	30.44	69.56
K-Sn-V/UiO-66	39.54	60.46

Table 3 V contents in different catalysts (at%)

Catalyst	V^{4+}	V^{5+}
V/UiO-66	35.47	64.53
K-V/UiO-66	25.04	74.96
Sn-V/UiO-66	29.51	70.49
K-Sn-V/UiO-66	27.05	72.95

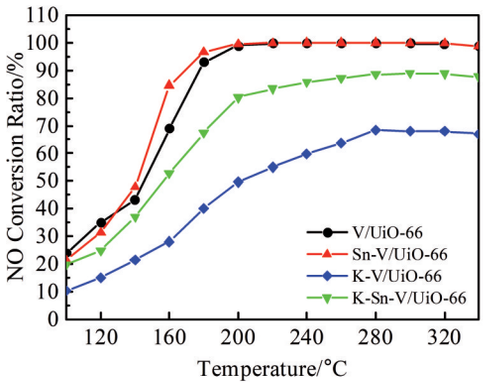

Fig.6 Denitration activity curves of different catalysts

$$V^{4+}\cdots NH_2+NO\rightarrow V^{4+}\cdots NH_2NO \quad (3)$$

$$V^{4+}\cdots NH_2NO\rightarrow V^{4+}+N_2+H_2O \quad (4)$$

$$2V^{4+}+1/2O_2\rightarrow 2V^{5+}+O^{2-} \quad (5)$$

$$2OH^-\rightarrow H_2O+O^{2-} \quad (6)$$

When K is loaded onto the catalyst, it reacts with the active sites, resulting in a significant decrease in NH_3 adsorption capacity. In addition, the redox performance of catalyst is reduced after K-poisoning, which affects the SCR reaction processes, such as NH_3 activation and NO oxidation, and ultimately leads to the catalyst deactivation[33].

The VO_x components on the surface of Sn-V/UiO-66 catalyst interact with other components, such as V-O-Sn and V-O-Zr, therefore improving the reducibility of VO_x components on the catalyst and increasing the proportion of V^{5+} components in the catalyst, which results in more Brønsted acid sites on the catalyst surface.

In addition, Sn^{4+} is highly acidic, and SnO_2 can quickly chemisorb NH_3 and form a coordination state with NH_2 on its surface. Therefore, SnO_2 can enhance the NH_3 adsorption capacity of catalyst, more NH_2 in the coordination state is generated, and the denitration efficiency of catalyst is improved. The total acid content of the poisoned K-Sn-V/UiO-66 catalyst is still higher than that of the V/UiO-66 catalyst, indicating that adding Sn can reduce the impact of K-poisoning on the surface acidity of the catalyst, lead to high acid content, and enhance the anti-alkali metal poisoning effects.

3 Conclusions

1) Compared with those of the V/UiO-66 catalyst, Sn-V/UiO-66 catalyst has smaller grain size, larger specific surface area, higher surface acid content, stronger redox capacity, and a large number of surface-active oxygen components. Sn-V/UiO-66 catalyst has excellent denitration efficiency, which is stable of nearly 100% at 180–340 °C.

2) The K-Sn-V/UiO-66 catalyst converts 80% NO_x, whereas the V/UiO-66 catalyst only converts 60% NO_x.

3) Potassium salts can cause catalyst poisoning, therefore decreasing the catalyst activity. The potassium salt weakens the interactions between the active components and the catalyst carrier and reduces the surface acidity and redox property of catalyst. The poisoned K-Sn-V/UiO-66 catalyst still maintains the excellent redox property and high acid content, presenting superb resistance against alkali metal poisoning.

References

1 Wu Yanxia, Liang Hailong, Chen Xin *et al. Rare Metal Materials and Engineering*[J], 2021, 50(12): 4256
2 Busca G, Lietti L, Rammis G *et al. Applied Catalysis B: Environmental*[J], 1998, 18(1–2): 1
3 Xiao Yong, Liu Zhenyu, Xing Xinyan *et al. The Chinese Journal of Process Engineering*[J], 2008, 8(3): 460 (in Chinese)
4 Wu Yanxia, Liang Hailong, Chen Xin *et al. Journal of Fuel Chemistry and Technology*[J], 2020, 48(2): 189 (in Chinese)
5 Madia G, Elsener M, Koebel M *et al. Applied Catalysis B: Environmental*[J], 2002, 39(2): 181
6 Went G T, Leu L J, Bell A T. *Journal of Catalysis*[J], 1992, 134(2): 479
7 Chen J P, Yang R T. *Applied Catalysis A: General*[J], 1992, 80(1): 135
8 Zhang Peng, Yao Qiang. *Coal Conversion*[J], 2005, 28(2): 18 (in Chinese)
9 Zheng Y, Jensen A D, Johnsson J E. *Applied Catalysis B: Environmental*[J], 2005, 60(3–4): 253
10 Chen J P, Yang R T. *Journal of Catalysis*[J], 1990, 125(2): 411
11 Peng Y, Li J H, Huang X *et al. Environmental Science & Technology*[J], 2014, 48(8): 4515
12 Lietti L, Forzatti P, Ramis G *et al. Applied Catalysis B: Environmental*[J], 1993, 3(1): 13
13 Kamata H, Takahashi K, Odenbrand C U I. *Journal of Molecular Catalysis A: Chemical*[J], 1999, 139(2–3): 189
14 Wang Junjie, Zhang Yaping, Wang Wenxuan *et al. Journal of Fuel Chemistry and Technology*[J], 2016, 44(7): 888 (in Chinese)
15 Shen Boxiong, Xiong Lixian, Liu Ting *et al. Journal of Fuel Chemistry and Technology*[J], 2010, 38(1): 85 (in Chinese)
16 Huang Zhiwei, Li Hao, Gao Jiayi *et al. Environmental Science & Thchnology*[J], 2015, 49(24): 14 460
17 Huang Zhiwei, Gu Xiao, Wen Wen *et al. Angewandte Chemie*[J], 2013, 152(2): 688
18 Li Chao, Huang Zhiwei, Liu Xiaona *et al. Chemical Communications*[J], 2019, 55(66): 9853
19 Wu Yanxia, Liang Hailong, Chen Xin *et al. Materials Reports* [J], 2021, 35(6): 6020 (in Chinese)
20 Zhang Yaping, Wang Longfei, Li Juan *et al. Chinese Journal of Catalysis*[J], 2016, 37(11): 1918 (in Chinese)
21 Li Shujian, You XIaochen, Sheng Zhongyi *et al. Chinese Journal of Environmental Engineering*[J], 2018, 12(8): 2231 (in Chinese)
22 Jiang Ye, Liang Guitao, Bao Changzhong *et al. Journal of China Uinversity of Petroleum*[J], 2017, 41(5): 139 (in Chinese)

23 Huang Lihua, Li Xue, Hua Jian. *Advanced Engineering Sciences* [J], 2019, 51(5): 185 (in Chinese)
24 Bao Qiang, Zhou Hao, Liu Jiancheng *et al*. *Journal of Zhejiang Uiversity* (*Engineering Science*) [J], 2015, 49(10): 1855 (in Chinese)
25 Nicosia D, Czekaj I, Krocher O. *Applied Catalysis B: Environmental*[J], 2008, 77(3): 228
26 Wang Dong, Wu Jingkun, Niu Shengli. *Journal of Fuel Chemistry and Technology*[J], 2015, 43(7): 876 (in Chinese)
27 Wu Yanxia, Wang Xianzhong, Liang Hailong *et al*. *Rare Metal Materials and Engineering*[J], 2021, 50(7): 2343
28 Hu P P, Schuster M E, Huang Z W *et al*. *Chemistry: A European Journal*[J], 2015, 21(27): 9619
29 Zhou Xuerong, Zhang Xiaopeng. *Chemistry*[J], 2015, 78(7): 590 (in Chinese)
30 Wang Lixia, Zhong Zhaoping, Zhu Lin *et al*. *Chemical Industry and Engineering Progress*[J], 2017, 36(11): 4064 (in Chinese)
31 Wu Yanxia, Liang Hailong, Chen Xin *et al*. *Environmental Protection of Chemical Industry*[J], 2016, 36(3): 321 (in Chinese)
32 Cao Jun, Yao Xiaojiang, Yang Fumo *et al*. *Chinese Journal of Catalysis*[J], 2019, 40(1): 95
33 Wang Dianer, Li Guobo, Li Chao *et al*. *Journal of Molecular Catalysis* (*China*)[J], 2019, 33(6): 508 (in Chinese)

掺杂Sn对V/UiO-66催化剂抗碱金属性能的影响

吴彦霞，陈玉峰，梁海龙，胡利明，王春朋
(中国建筑材料科学研究总院 陶瓷科学研究院，北京 100024)

摘　要：采用浸渍法，以UiO-66为载体，制备了V/UiO-66及改性Sn-V/UiO-66催化剂，并对催化剂的碱金属钾中毒进行了模拟，探讨了钒钛催化剂的反应机理和失活机理。结果表明，K负载后催化剂的晶型变化不大并且催化剂比表面积的变化呈现不规律波动。负载了碱金属以后，催化剂的金属氧化还原性能和表面酸量迅速降低，这是催化剂活性降低的主要原因。添加Sn能够增强VO_x与其他组分的相互作用，进而提高VO_x的可还原性及V^{5+}的占比，使Sn-V/UiO-66催化剂表面的VO_x提供更多的酸性位点。中毒后的K-Sn-V/UiO-66催化剂仍然具有较高的总酸量和较强的氧化还原性，表明Sn-V/UiO-66催化剂具有优异的抗碱金属中毒能力。

关键词：UiO-66催化剂；催化脱硝；NH_3-SCR；改性

作者简介：吴彦霞，女，1988年生，博士生，工程师，中国建筑材料科学研究总院陶瓷科学研究院，北京 100024，电话：010-51167727，E-mail：wuyanxia@cbma.com.cn